Wavefield synthetics in 3D and fully automatic event locations

Eystein S. Husebye and Bent O. Ruud
Institute of Solid Earth Physics, University of Bergen, Norway

AFOSR Grant F49620-94-1-0278

Abstract

The research under this contract have mainly been along two directions: (1) three-dimensional (3D) finite difference (FD) modeling of scattering from free surface topography, and (2) near real time event location using only seismogram envelopes from local networks. In (1) we have simulated scattering from teleseismic P-waves using a plan vertical incident P-wave and real topography from a 40 × 40 km area centered at the NORESS array in south-eastern Norway. Snapshots and synthetic seismograms of the wavefield show clear conversion from P to R_g (short period fundamental mode Rayleigh) waves in an area of rough topography approximately 10 km east of NORESS. This result is consistent with numerous observations.

In (2) a new method is described for automatic epicenter locations in near real time using short period z-component data from local seismograph networks. The original waveform data is bandpass filtered, 'STA envelope' parameterized and then resampled at a rate of 2 Hz. The physical principle invoked for epicenter determinations is that of constructing the space-time image of a source in the gridded network area on the basis of P- and S-wavelet intensities. Since such intensities for a stratified half space is almost model independent we did not bother to use local travel time tables nor crustal models. The latter information is naturally needed for precise origin time estimates. The method is robust because and to our surprise, P- and S-intensities (low frequency wavelets) vary smoothly (1D) with distances at least out to 700 km. Compared to conventional event location approaches, we bypassed tasks like signal detection, phase identification and phase association - in essence we aim for joint *event* detection and location. The method has been very convincingly tested on Italian, German and Norwegian network data off-line but has not been adapted to a real time operational environment nor attempted extended to teleseismic recordings. In the former case we see no principal problems and besides computational requirements can be handled by a PC machine. The essence of our automatic epicenter location scheme is the potential for fast (3-4 min), effective and low-cost exploitation of CTBT relevant monitoring information from the very many local networks deployed in most continental areas. In the future we foresee that local network Hubs may inform the IDC of a CTBT treaty about incoming P-waves at teleseismic located stations and arrays from specific sources at given locations. Also, the ever increasing use of Internet for seismic data exchange may at least partly move CTBT seismic monitoring into the seismological community sphere and perhaps partly into the public domain.

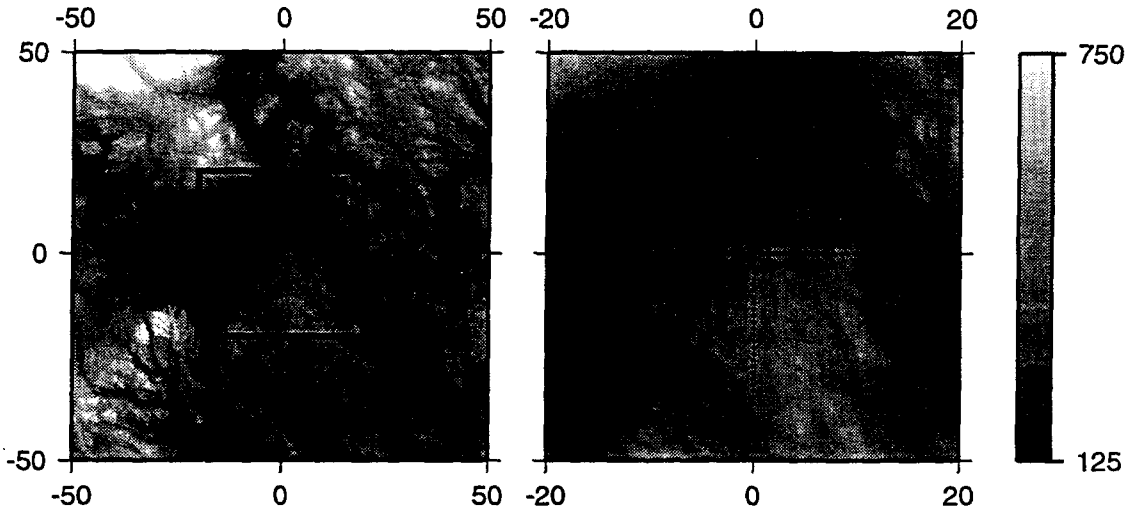

Figure 1: Leftmost section shows the topography in an 100 × 100 km area centered at the NORESS array. The innermost 40 × 40 km was used in the modeling experiment. The dotted lines shows the positions of the receivers in the two profiles and the circle outlines the NORESS array. Labels are in kilometers and elevations are in meters above mean sea level. The black area is Lake Mjøsa (123 m above sea level).

1 Objective

The main goal of the basic seismological research performed under this contract is to improve our understanding of wave propagation and scattering phenomena for local and regional distance travel paths. The tool used here is numerical simulations through the very general and powerful, but computationally demanding, finite difference technique.

Another research goal is aimed at exploiting the information potential of local network recordings in the context of CTBT monitoring. the first step here is the development of a fast, cost-efficient method for automatic event locations using such network data. To ensure robustness, conventional analysis tasks like signal detection, phase identification and association were avoided.

2 Basic research results (B.O.Ruud and S.Hestholm)

2.1 3D FD modeling of scattering from topographic relief

The scattering of teleseismic P wave energy into R_g have been extensively studied and documented using data from the NORESS array in south-eastern Norway (Bannister et al, 1990; Gupta et al, 1993; Hedlin et al, 1991, 1994). For our 3D FD modeling experiments we have obtained digital elevation data for an area of 100 × 100 km centered on the NORESS array (Fig. 1). Due to the huge computer memory requirements of 3D FD methods, we have so far been restricted to a model of size 40 × 40 × 35 km with 0.2 km sampling.

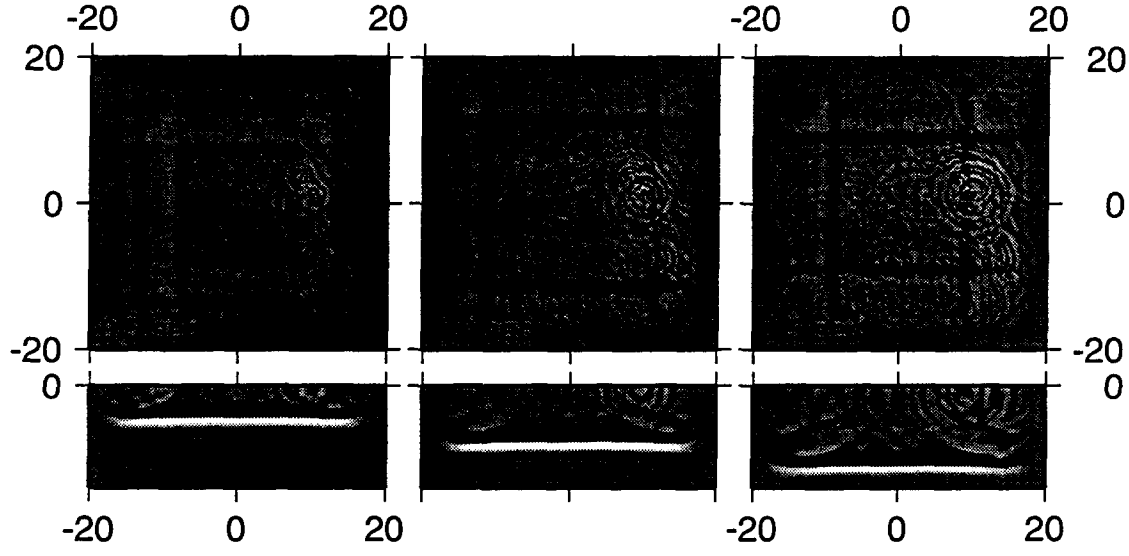

Figure 2: Snapshots of the vertical component of the particle velocity. The upper snapshots are horizontal sections at the free surface and the lower snapshots are vertical sections along a west-east profile through the center of the model. The time in the lower left corner of each horizontal section is the time from when the plane vertical incident P-wave was reflected from the surface. The straight wavefronts parallel to the model boundaries are artificial reflections from the absorbing boundaries. These artificial reflections are seen also in the vertical sections. Note the strong scattering source located at Bronkeberget (2 km N, 10 km E) which is also highly prominent in real record analysis (Bannister et al, 1990).

The method used to implement free surface topography in the 3D FD code is an extension of the 2D method described by Hestholm and Ruud (1994). In all the examples shown here the incoming wave is a vertical incident plane P-wave simulating a teleseismic short period P-phase. The center frequency of the Ricker wavelet is 2.5 Hz, the P-wave velocity of the homogeneous medium is 6.0 km/s and the Poisson's ratio is 0.25. The absorbing boundary condition used along the sides and bottom of the model is the so called 'exponential damping' technique.

The main problem encountered in our test runs was instabilities which started near the surface in areas of steep and rough topography. The instabilities appear as surface waves of exponentially increasing energy which slowly propagate out from the starting points. The first modeling attempt with unsmoothed real topography gave very unstable results (infinite amplitude) within a second after the wave front reached the surface. In our next attempt the elevations were first multiplied by 0.5 in order to reduce the topography. The results were stable and this is also consistent with previous 2D FD modeling results. Also in the latter case an west-east profile running through NORESS was unstable with real topography but stable with half elevations. Snapshots of the wavefield (vertical component of the particle velocity) are shown in Fig. 2. A dominant feature of the snapshots is the low-frequency/long-wavelength artificial reflections from the absorbing boundaries. Although the exponential damping technique is the most efficient absorbing boundary method we have tested, the case of an wave incident at an angle of 90° with the boundary is the most difficult one. Fortunately, the artificial reflections are frequency dependent, with longer wavelengths than most of the surface waves scattered by the topography, and can therefore be

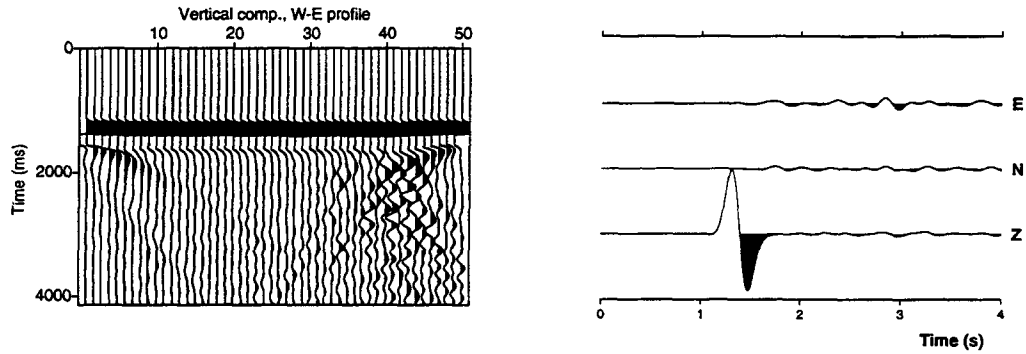

Figure 3: Seismograms extracted at the free surface of the model. Left section shows the vertical component of the particle velocity along a 30 km long west-east profile through the center of the model. The right section shows 3-component seismograms from a receiver 3.6 km east of the center.

removed by filtering and image processing techniques. As seen from Fig. 2 the scattered surface waves appear to radiate out from secondary point sources which coincide with areas of high topographic gradients (Fig. 1). The dominant scattering points are along the steep valley side east of 'Bronkeberget' about 10 km east of NORESS (Bannister at al., 1990). Also in seismograms from the west-east profile the P-to-R_g scattering from this area is clearly seen (Fig. 3).

2.2 Recommendations and future plans - 3D FD synthetics

Even for small scale experiments 3D FD synthetic wavefield analysis provide, as demonstrated here, improved insight and a better understanding of surface scattering phenomenon. We find it particularly gratifying that the strong P-to-R_g scattering from the Bronkeberget hill, observed by Bannister et al. (1990) through analysis of NORESS recordings, can be realistically synthesized. Another interesting feature is that for certain spatial low-frequency variants of the local NORESS topography the R_g wave propagation seems to change abruptly over relatively small distances. Probably, this is due to strong directionality dependence of the scattering from some topographic features. Such wavefield characteristics are sometimes observed in NORESS and GERESS recordings – at some sensors the R_g-phase is prominent while hardly visible at nearby sensors less than a kilometer away. In other words, also small scale crustal features may contribute to blocking effects as often observed for R_g- and L_g-phases. Many of such wave field phenomena are out of range for 2D FD synthetic experiments hence our emphasize on continuous research efforts on 3D synthetic simulation of crustal wave field propagation.

Recently, we have modified the code to run on parallel computers and we are now in the testing stage. Future directions of our research will be to increase the model size to also include the scattering areas SE of Lake Mjøsa. Furthermore, in order to compare directly with NORESS recordings it is necessary to allow for non-vertical incident waves and to use source time functions derived from teleseismic P beams. Although the physical dimensions of 3D models still will be quite small compared with 2D FD models, the use of parallel computer technology opens new avenues to study of 3D scattering phenomena in fields like random media and corrugated interface scattering.

3 Automatic event location using local network data

(G.A. Ryzhikov, M.S. Biryulina and E.S. Husebye)

As a preamble to deciding on a local event location strategy we attempted to formulate sort of 'boundary conditions' for approach. Firstly, to tie the analysis to the parameterized waveforms make sense also scientifically because signal waveforms are dissimilar for station separations exceeding a few kilometers. Likewise, an approach in principle similar to conventional ones including signal detection, phase identification and phase association was rated unattractive because corresponding parameters extraction in an automatic mode is unlikely to be robust (Ruud et al, 1993). Finally, for local events there is no need to ignore a priori information embedded in the event records namely the presence of the two P- and S-wave modes and with the latter being relatively energetic. Incorporating amplitude information would naturally reduce the severity of the phase association problem due to fast signal amplitude decay with epicenter distance.

From the above considerations, we formulated the following epicenter location strategy:

1. Analysis restricted to parameterized waveform data say tied to rms or to the STA detector parameter definition (sampling rate 0.5-1.0 sec)
2. Extraction of 1D (distance dependence only) signal attributes to ensure robustness of analysis.
3. A grid search approach giving an option for including a priori information in on-line analysis.
4. Epicenter location criteria based in minimizing differences between observed and expected seismic signal attribute features.
5. 'Expected' attributes to be anchored in seismic wave propagation theory.

3.1 Theory - event localization strategy realization

Out of the various task listed above, that of transforming the original waveforms or parameterized waveform records in such a manner that distinct signal attributes could be extracted reliably, proved difficult to realize in practise. In particular the increasing scattering contribution to the observed wavefield with time tend to obscure distinct signal features for larger ($\Delta > 300$ km) epicenter distances. With the failure of our empirical experiments in minimizing distinct signal attributes, we examined many works on wave propagation in stratified media for a clue to this problem (e.g., see Brekhovskikh 1960, Aki and Richards 1981, Kennett 1983, Flatte et al, 1979). On this, presumably adequate theoretical basis, we proceeded in a manner reminiscent of Chap.3 and 4 in the Aki and Richards book. In other words, the starting point being the far field displacement for a time-space distributed source in an inhomogeneous media expressible as:

$$\varphi_i(\mathbf{x},t) = G_{ij}(\mathbf{x},\mathbf{x}';\, t-\tau)s_i(\mathbf{x}',t) \qquad (1)$$

where φ_i is the ith displacement component at location $\mathbf{x}$ ($\mathbf{x} = \{x_1, x_2, x_3\} \stackrel{\text{def}}{=} \{\mathbf{r}, z\}$), $\mathbf{r}$ being the free surface location and z is depth) and time t; G_{ij} is the Green operator (tensor function) and s_i is the body force equivalent at position $\mathbf{x}'$ and time τ. The Green function is complicated, depending essentially on an infinite number of medium parameters and as such not attractive in

a real time analysis environment. Hence we rewrite eq. (1) for an isotropic stratified medium in the following form:

$$\varphi^0 = G^0 s \tag{2}$$

with index zero signifying the simplified medium. We may rewrite the general Green function in terms of that for the simplified media, namely

$$G = G^0 + \delta G \tag{3}$$

where $G^0 = G^0(|\mathbf{x} - \mathbf{x}'|;\, t - \tau)$. Introducing the Lamé operator L on G:

$$LG = \delta(\mathbf{x} - \mathbf{x}')\delta(t - \tau) \tag{4}$$

where the L-operator in time-frequency representation is of the form:

$$L = -\rho\omega^2\delta_{ik} - \partial_j[c_{ijkl}\partial_l] \tag{5}$$

with ρ= density, δ = Kronecker delta, ω = angular frequency and c = elasticity tensor. Using the L -operator, we have for δG (eq. 3):

$$\delta G = -G^0(L - L^0)G = G^0 V G \tag{6}$$

where the potential $V = L^0 - L$. Obviously, seismic waveforms vary rapidly between stations so preferences are for wavefield intensity or amplitude square measures, that is

$$\varphi\varphi^* = GG^* ss* \tag{7}$$

where G^* stands for the operator being adjoint to G. Inserting eqs.(2), (3), and (6) in eq. (7) we get

$$\overline{\varphi\varphi^*} = \overline{\varphi^0\varphi^{0*}} + G^0 G^{0*}\overline{VV^*\varphi\varphi^*} \tag{8}$$

where the overline imply averaging over two separate recording positions and operator $\overline{VV^*}$ is supposed to be essentially nonlocal. Note that equation (8) describes wavefield intensities taking into account that we have omitted the expression $\delta(\mathbf{x}_1 - \mathbf{x}_2)\delta(t_1 - t_2)$ for equation (8); all terms should be multiplied by the expression.

Now, recalling, that our 'target zone' is the free surface we are interested in describing of energy flux in lateral direction, with G^0 describing the propagation in a stratified halfspace with smooth perturbations. V can be modeled as an ensemble of random functions with *lateral* radius of correlation being dominant, which gives the wave propagation in terms of adiabatically perturbed normal modes. This means that propagation in lateral direction $\mathbf{r} - \mathbf{r}^*$ ($\mathbf{r}^*$ is epicenter) can be treated in terms of a parabolic wave equation, and eq. (8) can be treated as an equation of evolution of intensity $w \stackrel{\text{def}}{=} \overline{\varphi\varphi^*}\delta(\mathbf{x}_1 - \mathbf{x}_2)\delta(t_1 - t_2)$. Physically, we have at this stage a simplified expression for wavefield intensity with the term $\overline{\varphi^0\varphi^{0*}}$ being the energy flux in an isotropic medium and the $\overline{VV^*}$- term giving diffusion of energy during propagation. Note, the propagation of an *impulse* signal in isotropic stratified half space has two main wavefield intensity components in a vicinity of the free surface: *P-primary*, or '3D-mode' and *S-secondary*, or principal '2D-mode', having specific group velocities, which are defined for the P-mode by turning points at depth $z > 0$ and for S-mode is caused by a turning point at depth $z = 0$ (Kennett, 1983). Now the difference $\Delta w = w - w^0$ between intensities in an inhomogeneous half space w and in an isotropic stratified one has to satisfy the diffusion equation:

$$\frac{\partial \Delta w(r,t)}{\partial r} = a^2 \frac{\partial^2 \Delta w(r,t)}{\partial t^2} \tag{9}$$

where a is the diffusion coefficient. Equation (9) gives the distance dependence of wavefield intensity for localized (point) source function.

Observationally, seismogram intensity may be of form of the STA detector (Ruud et al,1993), and we want to minimize the differences between observed u and modeled w wavefield intensities, namely to find w such that

$$\mathcal{M} = \langle u - w | u - w \rangle \rightarrow \min \tag{10}$$

where $u = \{u(\mathbf{r}_n, z = 0;\ t) = u(\mathbf{r}_n, t) = u_n | n = 1, 2, \ldots, N\}$, where $\mathbf{r}_n$ is the n-th station, N is number of stations and $w = w(|\mathbf{r} - \mathbf{r}'|, z = 0;\ t - \tau)$, and

$$\langle u | w \rangle \stackrel{\text{def}}{=} \frac{1}{N} \sum_{n=1}^{N} \int_{\Delta t} u(\mathbf{r}_i, t) w(\mathbf{r}_i, t) \mathrm{d}t$$

We may write a model for observations u_i on the base of modeled w (eq.(8)) in an approximate manner by assuming linearity in terms of intensities, that is:

$$w_n = w_n^0 + \delta w_n = Wf + \delta w_n \tag{11}$$

where $W = G^0 G^{0^*}(|\mathbf{r}_n - \mathbf{r}'|, z = 0; t - \tau))$, $f = f(\mathbf{r}', t)$ is source function squared; $\delta w_n = \delta w(\mathbf{r}_n, t)$ is an error term, which can be interpreted as a random realization of Δw with covariance operator $C_w = \overline{\delta w_n \delta w_n} = \exp\{a^2 r_n \partial_t^2\}$ (eq.(9)). The equation $w_n^0 = Wf$ is similar to eq.(1) except that displacement is replaced by wavefield intensity and at that in a simplified manner. From eq.(11) we can estimate the source intensity $f(\mathbf{r}', t)$:

$$\hat{f} = (W^* C_w^{-1} W + \alpha \mathrm{I})^{-1} W^* C_w^{-1} u \tag{12}$$

where α is positive parameter of regularization. Using a RT-approximation (Ryzhikov and Troyan 1992 a,b) and presuming linearity of w with respect to f, we may rewrite eq.(11) for dimensionless values $\tilde{f} = f/f_{\max}$ and $\tilde{u} = u/u_{\max}$ in the following form:

$$\tilde{f}(\mathbf{r}', \tau) = \frac{\langle \tilde{W_{\mathbf{r}',\tau}} \mid \mathcal{F}\tilde{u} \rangle}{\langle W_{\mathbf{r}',\tau} | W_{\mathbf{r}',\tau} \rangle + \alpha} \tag{13}$$

where observed data $\tilde{u}$ are filtered by operator $\mathcal{F} = exp\{-(1/2)a^2 r_n \partial_t^2\}$ (Fig. 4c) and the unit intensity source response $\tilde{W_{\mathbf{r}',\tau}} = W(|\mathbf{r} - \mathbf{r}''|, t - t')\delta(\mathbf{r}'' - \mathbf{r}')\delta(t' - \tau)$ (an eq.(1) analogy). Albeit $\hat{f}$ may be used as an event magnitude measure, we prefer to work with normalized observational data. This ensures that corresponding source intensity function $\tilde{f}$ varies between 0 to 1.0 and plays the role of correlation between the real and virtual source intensity functions. It allows us to introduce the *source image* function:

$$\psi(\mathbf{r}', \tau) = \exp\{\sigma^{-2}[\tilde{f}(\mathbf{r}', \tau) - 1]\} \tag{14}$$

where $\tilde{f}(\mathbf{r}', \tau)$ is the normalized value of f in eq.(13). The entropy of source image contrast (EnIC), defined by Biryulina and Ryzhikov (1995) is :

$$\mathcal{E}_\psi(\tau) = -\int_\Omega \mu(\mathbf{r}', \tau)) \ln \mu(\mathbf{r}', \tau)) \mathrm{d}\mathbf{r}' \tag{15}$$

via a pseudo-probability density function $\mu(\mathbf{r}', t) = (\partial_{\mathbf{r}'}\psi)^2(\mathbf{r}', \tau) / \int_\Omega (\partial_{\mathbf{r}'}\psi)^2 \mathrm{d}\mathbf{r}'$. The attractive feature of the EnIC is that of beig a very good measure for detecting a single impulse-like seismic event. A more detailed theoretical basis of this epicenter location scheme is given by Ryzhikov, Biryulina and Husebye (1995, in preparation)

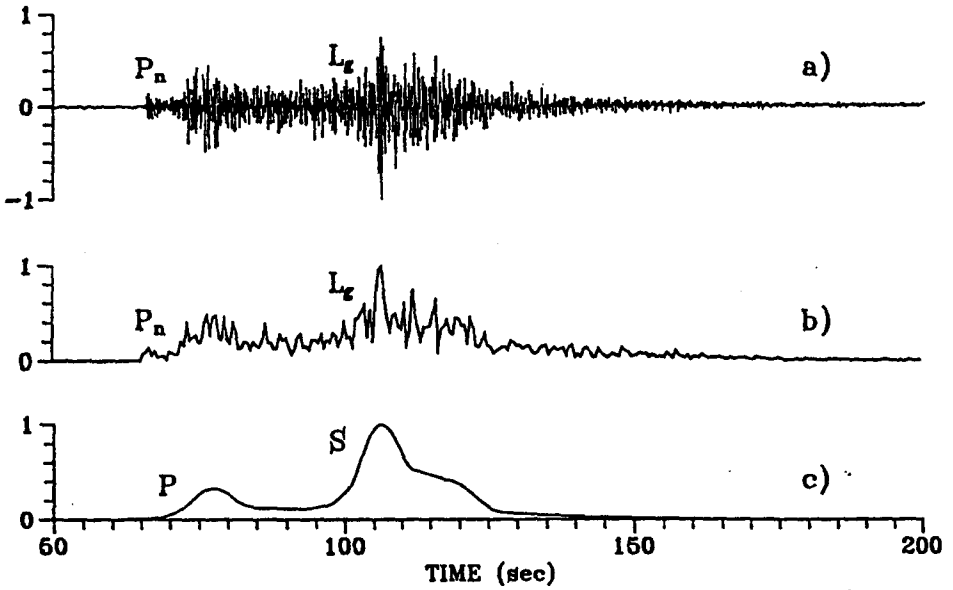

Figure 4: Local event record for the Italian station FVI at an epicenter distance of 240 km (date 11/02/95 - Table 1). a) Original waveforms after 2 - 4 Hz bandpass filtering; sampling rate is 50 Hz. b) Parameterized version of the (a) waveform subjected to a simple non-overlapping short-term-average 'envelope' transform; sampling rate is 2 Hz. c) P- and S-intensity wavelets derived from the parameterized waveforms shown in (b). The peak of these wavelets as a function of distance (Fig. 5) are the only information used in our automatic location scheme. Basic seismic network traces used in analysis is the (b)-type parameterized waveforms which are easily produced in situ. Note, we have for convenience used the classical P- *primary* and S-*secondary* notations for the intensity wavelets in (c) and *with no relation* to corresponding analyst phase notations. The wavefield counterparts of the P- and S-intensity wavelets are given in eq.8.

3.2 Event location exercise using Italian, German and Norwegian data

We requested short period (z-component) STA transformed data from 3 local networks and in this respect as implied above did not bother about instrument responses, local travel time tables, and crustal models. In case of the German data we only had at hand station coordinates and the corresponding recordings. The various analysis steps were as follow:

1. Band pass filtering; 2-4 Hz pass band for SNR enhancement. The initial STA-transforms of waveforms was (sampling rate 0.5 sec, no overlap): $\mathrm{STA}^2 = \frac{1}{K}\sum_k \varphi_k^2$
2. Derive model for P- and S- mode intensity as a function of distance. Analysis step (1 and 2) is illustrated in Figures 4 and 5. Initially we used Fig. 5a for Germany.
3. Estimating minimum of entropy of source image contrast in time (see Fig. 6 for visualization)
4. Knowing the minimum of entropy time we searched the grid for the most probable location - our choice of epicenter locations (Fig. 7). In Table 1 we list reference epicenter locations (bulletins) and relative positions of our automatic locations.

The following comments apply; our location scheme is tied to epicenter determinations from which we could accurately compute origin time for a preset focal depth and local travel time tables. Event and magnitudes are easily derived from the STA-parameters using the Mendi and Husebye (1994) method.

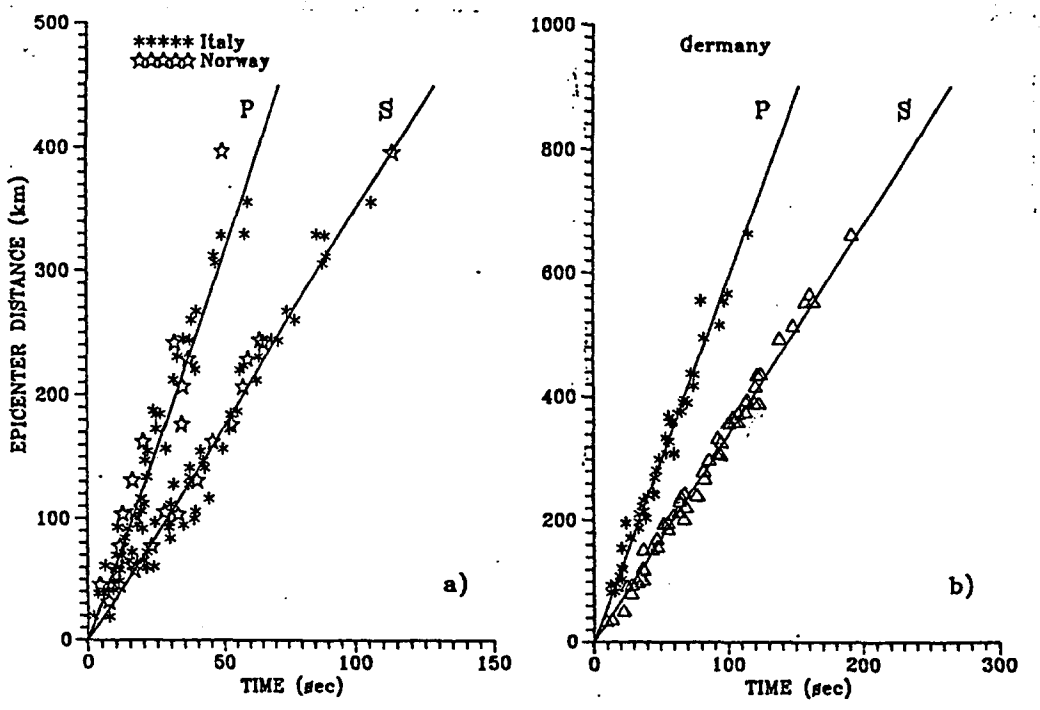

Figure 5: P- and S-intensity wavelet travel times for Italian, Norwegian (a) and German (b) network recordings. The corresponding wavelet velocities are 6.3 km/s and 3.5 km/s for (a) and 5.9 km/s and 3.4 km/s respectively for (b).

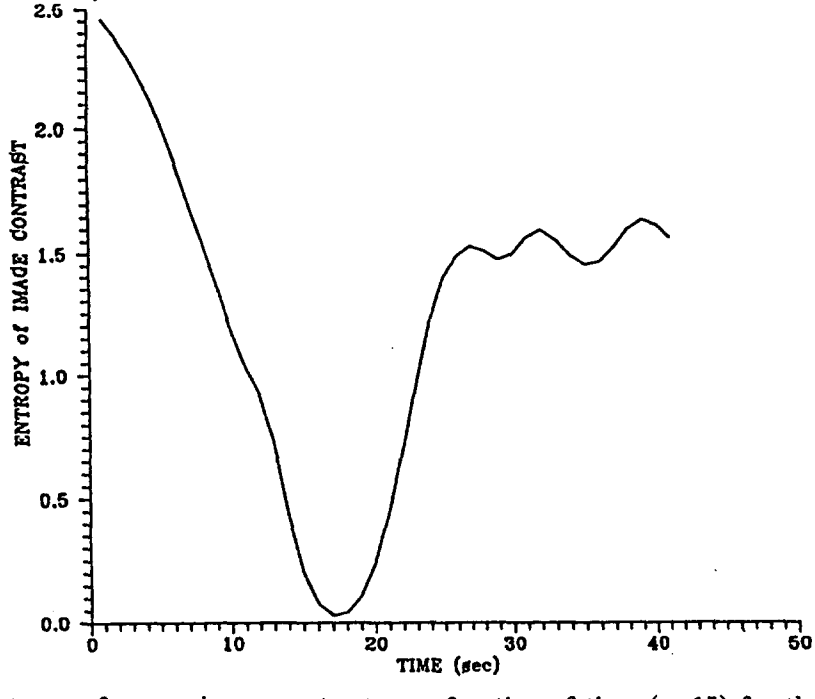

Figure 6: Entropy of source image contrast as a function of time (eq.15) for the Italian event of 11/02/95 (Table 1). Note the clear functional minimum at 17 sec being typical of real event detections. The corresponding spatial distribution of the source image function over the spatial sampling area is shown in Fig.7 .

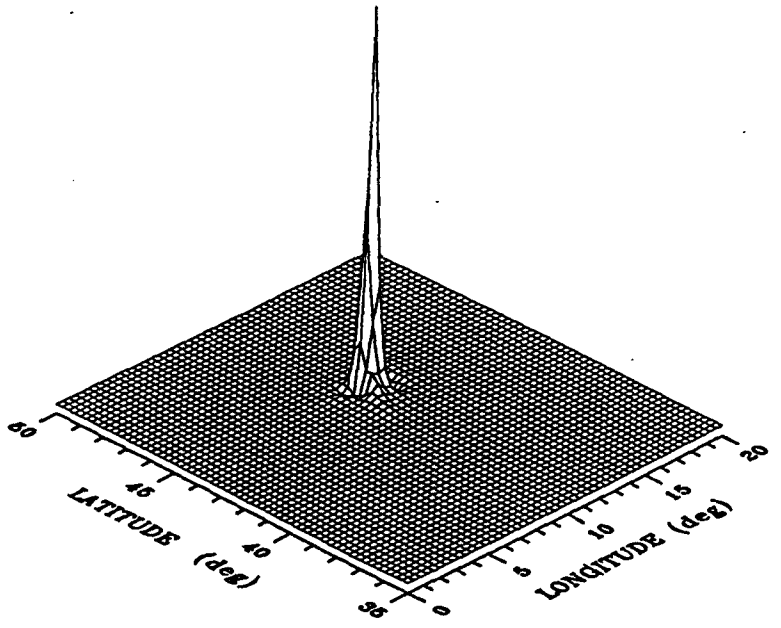

Figure 7: The spatial distribution of the source image function for the Italian event of 11/02/95 at time 17 sec coinciding with the entropy minimum in Fig. 6. The spatial position of the functional maximum in eq.(14) is taken as the epicenter coordinates (see listings in Table 1, where comparisons are made with bulletin locations).

Date	*Bulletin data*		*Deviation*		*Date*	*Bulletin data*		*Deviation*	
d/m/y	*LatN*	*LonE*	*ΔLat*	*Δ Lon*	*d/m/y/*	*LatN*	*LonE*	*ΔLat*	*Δ Lon*
GERMANY					*ITALY*				
30/07/94	**51.45**	**11.43**	**0.06**	**0.02**	**11/12/94**	**37.81**	**15.61**	**-0.01**	**-0.27**
17/09/94	**51.45**	**10.50**	**0.08**	**0.13**	**02/01/95**	**40.82**	**15.34**	**-0.15**	**-0.10**
04/12/94	**50.25**	**12.44**	**0.23**	**-0.12**	**04/01/95**	**44.87**	**7.36**	**-0.11**	**-0.26**
16/01/95	**50.83**	**6.35**	**-0.05**	**0.11**	**11/02/95**	**44.28**	**11.50**	**0.01**	**-0.16**
22/01/95	**48.18**	**8.75**	**-0.11**	**-0.13**	**18/02/95**	**39.14**	**16.45**	**0.11**	**-0.23**
10/03/95	**50.79**	**6.35**	**0.01**	**0.04**	**26/02/95**	**44.49**	**12.08**	**-0.05**	**0.12**
24/03/95	**47.79**	**8.83**	**-0.36**	**-0.64**	*NORWAY*				
30/03/95	**51.46**	**10.40**	**-0.29**	**0.39**	**26/08/93**	**59.05**	**5.77**	**0.02**	**0.24**
03/06/95	**51.49**	**16.20**	**0.18**	**-0.16**	**26/08/93**	**61.11**	**4.07**	**-0.10**	**0.18**
07/06/95	**51.48**	**16.20**	**0.22**	**-0.12**	**13/09/93**	**66.34**	**5.67**	**-0.34**	**0.68**

Table 1: Comparisons between event locations as reported in local bulletins and those obtained using our automatic location scheme - differences are mostly small. The few exceptions in this regard are events located outside or on the periphery of the German (ca 8 stations used) and Norwegian (ca 6 stations used) network areas where the epicenter resolution is relatively poor for any location method. (ca 20 stations used from Italian network area)

3.3 Research accomplished

An automatic and robust method for event location using local network data has been developed. It is easily adapted to any local network area - no need for overly detailed structural information. It is economical on two accounts; (i) In situ sampling rate is 0.5 sec or lower so minimal data transfer costs (ii) Analyst interference with finalized event solutions is likely to be minimal since we bypass conventional not so robust analysis steps like signal detection, phase identification and phase association. Event detectability, not excessively tested, is likely to be good as the method 'focuses' on maximum P-and S-wave- mode intensities and not often weak phase onsets (Fig. 4)

3.4 Recommendations and future plans

The main recommendation is that the information potential of local seismograph networks in the context of CTBT monitoring should be exploited to an extent far greater than currently under consideration. The novel method of event location presented provides one avenue for achieving a better, faster and more effective monitoring environment. Note, our approach is based on existing network instrumentation and perhaps most important does not incure excessive data transmission costs.

Options for further method refinements are by no means exhausted; future research topics are better handling of short distance records (P/S interference/overlap), interfering events and naturally method adaptation to a real time operational environment. Future plans also include efforts to extend methodology to teleseismic recordings and most challenging if source type identification estimates can be included for earthquake magnitudes above 3 and naturally for the many stationary mining and quarry sites.

References

Aki, K. and Richards, P.G., 1980. *Quantitative Seismology: Theory and Methods*, Vol. 1, W.H. Freeman, San Francisco.

Biryulina, M. and Ryzhikov, G., 1995. Rytov-Born decomposition in 3-D reflection seismics, in *Extended Abstracts of EAEG and EAPG 57th Conference and Technical Exhibition*, Vol.1, EAGE, Glasgow.

Brekhovskikh, L.M., 1960. *Waves in Layered Media*, Academic Press, New York.

Bannister, S.C., Husebye, E.S., and Ruud, B.O., 1990. Teleseismic P-coda analyzed by three-component and array techniques – deterministic location of topographic P-to-R_g scattering near the NORESS array, *Bull. Seism. Soc. Am.*, **80**, 1969-1986.

Flatte, S.M., Dashen, R., Munk, W.H., Watson, K.M. and Zachariasen, F.,1979. *Sound Transmission Through a Fluctuating Ocean*, Cambridge University Press, New York.

Gupta, I.N., Lynnes, C.S., and Wagner, R.A., 1993. An array study of the effects of a known local scatterers on regional phases, *Bull. Seism. Soc. Am.*, **83**, 53-63.

Hedlin, M.A., Minster, J.B. and Orcutt, J.A., 1991. Beam-stack imaging using a small aperture array, *Geophys. Res. Lett.*, **18**, 1771-1774.

Hedlin, M.A., Minster, J.B., and Orcutt, J.A., 1994. Resolution of prominent crustal scatterers near the NORESS small-aperture array, *Geophys. J. Int.*, **119**, 101-115.

Hestholm, S.O. and Ruud, B.O, 1994. 2D finite difference elastic wave modeling including surface topography, *Geophysical Prospecting*, **42**, 371-390.

Kennett, B.L.N.,1983. *Seismic Wave Propagation in Stratified Media*, Cambridge University Press, Cambridge.

Mendi, C.D. and Husebye, E.S., 1994. Near real time estimation of magnitudes and moments for local seismic events, *Annali di Geofisica*, **37**, 365-382.

Ruud, B.O., Lindholm, C.D. and Husebye E.S., 1993. An exercise in automating seismic record analysis and network bulletin production, *Bull.Seism.Soc.Am*, **83**, 660-679.

Ryzhikov, G.A. and Troyan, V.N., 1992a. Diffraction tomography. Part 1: Construction and interpretation of tomography functionals, in *Proceedings of Russian - Norwegian Oil Exploration Workshop II*, Voss, Published by Norsk Hydro A/S, Bergen, Norway.

Ryzhikov, G.A. and Troyan, V.N., 1992b. Diffraction tomography. Part 2: Reconstruction algorithm with statistical regularization, in *Proceedings of Russian - Norwegian Oil Exploration Workshop II*, Voss, Published by Norsk Hydro A/S, Bergen, Norway.

Ryzhikov, G.A., Biryulina, M.S. and Husebye E.S., 1995. Automatic local event location excluding signal detection, phase identification and association, *in preparation.*